# Tracks of Symmetric Top Molecules in Hexapole Electric Fields

**Roger W. Anderson**†

*Chemistry Department, University of California, Santa Cruz, California 95604 and Zentrum für Interdisziplinäre Forschung, Universität Bielefeld, Bielefeld, Germany*

*Received: April 16, 1997; In Final Form: June 13, 1997*⊗

The trajectories of symmetric top molecules are computed in hexapole electric fields. The transmission of a hexapole for linear Stark effect focusing is compared with that due to the exact interaction of the electric field with the symmetric top molecule. The use of the exact interaction in place of the linear Stark effect produces significant changes in the position and shape of the transmission peaks. Focusing curves are also calculated assuming the Stark effect calculated to second order. The nuclear quadrupole−electric field gradient interaction is found to significantly affect the focusing of $CH_3I$, and it is possible to produce a beam of rotational state selected and partially spin polarized $CH_3I$. The focusing for the usual experimental hexapole composed of cylindrical rods is compared with the focusing for an ideal hexapole, and a finite difference technique is used to determine the cylindrical rod radius that will provide the best approximation to an ideal hexapole field. This best rod radius is 0.565 of the hexapole radius, and focusing curves are shown for this choice of rod radius. A computer program to calculate trajectories for experimental hexapole arrangements with exact Stark interactions is available.

## 1. Introduction

It has been known, for more than 40 years,[1] that symmetric top molecules can be focused by means of the first order Stark effect in hexapole electric fields, and the first experimental confirmations of the technique occurred more than 30 years ago.[2] There have been many applications of this hexapole focusing technique in the intervening years, and the same physics that allows focusing of specific $|JKM\rangle$ states also allows the specification of the orientation of the dipole moment (symmetry axis) of the symmetric top molecules. This observation has allowed exploration of steric effects in bimolecular gas phase reactions (for reviews see refs 3−7) and direct determination of orientation by photodissociation[8,9] and electron diffraction.[10,11]

However, linear Stark focusing is an approximation that is valid only for hexapole electric fields that are not too large, for molecules without large hyperfine interactions, and for ideal hexapole fields. Inclusion of these complicating effects is likely to alter the position, shape, and size of the peaks in the focusing curves. In this paper we investigate the effects of higher order terms in the Stark effect, hyperfine interactions, and nonideal hexapoles. This work is the first systematic investigation of these focusing complications, although several other authors have addressed aspects of the problem. The focusing effects of the second order Stark effect has been studied recently,[12] and empirical attempts have been made to account for higher order Stark effects.[13,14] Bulthuis *et al.*[15,16] have explored the effect of hyperfine interactions on the degree of orientation that can be achieved with a molecule such as $CH_3I$, but they do not investigate the effects of hyperfine interactions on focusing. Several papers have proposed or used different methods to experimentally approximate hexapole fields, but none have presented trajectories for symmetric top molecules in the approximate hexapole fields. The UCLA hexapole experiments use specially machined electrodes that closely approximate the ideal hexapole equipotentials[17,18] but most of the hexapole experiments use cylindrical rod approximations to hexapole fields where the radius of the rods, $\rho_0$, is half of the hexapole radius, $r_0$ (half of the distance between the inside surfaces of the diametrically opposed rods). This choice for the rod radius will make the radii of curvature of the electric potential and the electrodes equal at the distance $r_0$.[5] Other workers have used $\rho_0$ to $r_0$ ratios of 0.667 [2] and 0.560.[19]

This paper will first explore the effects of higher order terms in the Stark effect. These will be done in two ways: effects on the force that the symmetric top molecules experience and consequences of the changes in the force for the trajectories. We will then show the effects of hyperfine interactions on forces and trajectories. Finally we will investigate trajectories in cylindrical rod approximations for hexapole electric fields.

## 2. Theoretical Preliminaries

**2.1. Interaction Energy.** Here we consider the interaction energy of polar symmetric top molecules in electric fields. We will look at this problem with several degrees of approximation or complexity. The Hamiltonian, **H**, for a symmetric top molecule in an electric field can be written as the sum of three terms:

$$\mathbf{H} = \mathbf{H}_0 + \mathbf{H}_\mathbf{Q} - \mu\cdot\mathbf{E} \tag{1}$$

The first term in eq 1 is the Hamiltonian for the field free symmetric top neglecting hyperfine interactions, and the second term describes the energy due to nuclear hyperfine interactions. This term is dominated by nuclear quadrupole moment−electric field gradient interactions. The third term describes the interaction of an applied electric field with the dipole moment $\mu$ of the molecule.

The interaction energy, $W$, of the molecule with an applied electric field is defined as

$$W = \epsilon_E - \epsilon_0 \tag{2}$$

where $\epsilon_E$ is the energy of a state with an applied electric field, **E**, and $\epsilon_0$ is the energy with no applied electric field. The energy of the molecule in an electric field can be estimated with first

† E-mail address: anderso@cats.ucsc.edu.

⊗ Abstract published in *Advance ACS Abstracts,* September 15, 1997.

S1089-5639(97)01313-3 CCC: $14.00 

order perturbation theory for weak fields, with second order perturbation theory for somewhat stronger electric fields, and with basis set expansions (exact treatment) for strong electric fields. In this paper we only consider electric fields that couple rotational states of the symmetric top, and we do not consider very strong electric fields (above 100 kV/cm) that may mix electronic states.

The actual calculation of the interaction energy depends on whether the hyperfine interaction term, $\mathbf{H_Q}$, is neglected or not. If the hyperfine term is neglected, then the eigenfunctions of $\mathbf{H}_0$ are described by the quantum numbers $J$, $K$, and $M$, which are the total angular momentum of the symmetric top, the projection of the total angular momentum on the unique principal axis of the top, and the projection of the total angular momentum on the space fixed $Z$ axis. The rotational eigenfunctions of a symmetric top are given as rotation matrices:[20]

$$|JKM\rangle = \left[\frac{2J+1}{8\pi^2}\right]^{1/2} D^{J*}_{MK}(\phi,\theta,\chi) \tag{3}$$

The rotational energy levels (diagonal elements) for $\mathbf{H}_0$ are $\epsilon_0 = hcBJ(J+1) + hc(A-B)K^2$, and the energy for increasing $K$ increases if the symmetric top is prolate ($A > B$) and decreases if the top is oblate ($A < B$). The rotational constants $A$ and $B$ are expressed in units of $cm^{-1}$.

The electric dipole−electric field interaction is easily written as $-\mu E \cos\theta = -\mu E P_1(\cos\theta)$, where $P_1$ is the Legendre polynomial of order 1. We will see with this observation that calculations will need evaluations of the matrix elements:

$$\langle J'K'M'|\, P_L|JKM\rangle = (-1)^{M'-K}[(2J+1)(2J'+1)]^{1/2}\begin{pmatrix} J & \mathrm{L} & J' \\ -M & 0 & M' \end{pmatrix}\begin{pmatrix} J & \mathrm{L} & J' \\ -K & 0 & K' \end{pmatrix} \tag{4}$$

where Wigner 3$j$ symbols are used.[20] These equations show that an obvious requirement for nonzero matrix elements is that $M = M'$ and $K = K'$.

The energy of the symmetric top in an applied field can be evaluated in different approximations. For first order perturbation calculations the interaction energy is given as the diagonal elements for each $|JKM\rangle$ state:

$$\mathrm{W}^{(1)} = -\mu E\langle JKM|P_1|JKM\rangle = -\mu E\frac{MK}{J(J+1)} \tag{5}$$

after explicit evaluation of the 3$j$ symbols. This shows that linear molecules without excited bending vibrations and diatomic molecules without unpaired electrons do not exhibit linear Stark effects, because in these cases $K = 0$. For molecules with a nonzero product $MK$ the interaction energy may either increase or decrease with increasing $E$, depending on whether the sign of the product is negative or positive.

The contribution to the interaction energy from second order perturbation theory is evaluated as[21]

$$W^{(2)} = \frac{1}{2}\mu E\Omega\left[\frac{[J^2-K^2][J^2-M^2]}{J^3(2J-1)(2J+1)} - \frac{[(J+1)^2-K^2][(J+1)^2-M^2]}{(J+1)^3(2J+1)(2J+3)}\right] \tag{6}$$

where $\Omega = (\mu E)/(hcB)$ is the commonly used ratio of the dipole−electric field interaction to the "rotational" energy $hcB$. The second order or quadratic Stark effect will be present for all symmetric tops and linear molecules.

The interaction energy due to the coupling of many $|JKM\rangle$ states by the electric field is easily calculated by expanding the wave function for the system in the electric field as

$$|KM\rangle = \sum_{J=\max(|K|,|M|)}^{J_{\max}} c_J|JKM\rangle \tag{7}$$

The energy eigenvalues and the eigenvectors of $\mathbf{H}$ are then found by diagonalizing the matrix of $\mathbf{H}$ in the $|JKM\rangle$ basis. Examination of eq 4 shows that this matrix will be tridiagonal because for $L = 1$ the angular momenta $|J - J'|$ must be less than or equal to 1. For our purposes the eigenvectors are not necessary because there are no avoided crossings in the spectrum of $\mathbf{H}$ as a function of $E$. However, the eigenvectors are important in other similar applications such as "brute force" orientation of molecules.[7] Here eigenvectors are important for fully quantifying the prepared Legendre moment ($\langle P_n(\cos\theta)\rangle$).

The nuclear hyperfine coupling term should not be neglected for symmetric tops that contain heavy atoms with nuclear quadrupole moments such as iodine. Quadrupole moments are possible whenever the nuclear spin, $I > {}^1/_2$, and in this case the calculation of the electric field interaction energy is somewhat more involved. It is convenient to work in the coupled basis where the rotational angular momentum $\mathbf{J}$ of the symmetric top is summed with the nuclear spin angular momentum $\mathbf{I}$ of the atom to produce a total angular momentum $\mathbf{F}$. The magnitude, $F$, takes all integral or half-integral values from $|J - I|$ to $|J + I|$ in unit steps. The eigenstates of $\mathbf{H}$ with nuclear coupling are characterized by the good quantum numbers $F$ and a projection $M_F$. The projection $M_F = M_J + M_I$, where $M_J$ is the projection of $\mathbf{J}$ and $M_I$ is the projection of $\mathbf{I}$. (In the discussion above about the case without nuclear hyperfine interactions, $M$ was used to denote $M_J$.) We see that the hyperfine coupling scrambles $J$ and its space fixed projection $M_J$. Since the nuclear hyperfine coupling does not mix values of $K$, the basis functions in the hyperfine case become $|\{JI\}KFM_F\rangle$, where the notation indicates that $\mathbf{J}$ and $\mathbf{I}$ couple together to form $F$.

For molecules without unpaired electrons the most important part of $\mathbf{H_Q}$ is the interaction of the nuclear quadrupole moment with the electric field gradient at the quadrupolar nucleus, and we neglect the much smaller nuclear spin−rotational coupling. The explicit form for the term in the Hamiltonian is[15]

$$\mathbf{H_Q} = \mathbf{V^{(2)}}\cdot\mathbf{Q^{(2)}} \tag{8}$$

where $\mathbf{Q^{(2)}}$ is the quadrupole tensor of the nucleus and $\mathbf{V^{(2)}}$ is the electric field gradient tensor at the nucleus.

The matrix elements of $\mathbf{H_Q}$ in the coupled basis are obtained with the aid of the following equation (after 5.71 [20]):

$$\langle\{J'I\}KFM_F|\mathbf{V^{(2)}}\cdot\mathbf{Q^{(2)}}|\{JI\}KFM_F\rangle = (-1)^{J+I+F}\begin{Bmatrix} J' & I & \mathrm{F} \\ \mathrm{I} & \mathrm{J} & 2 \end{Bmatrix}\langle J'K||V^2||JK\rangle\langle I||Q^2||I\rangle \tag{9}$$

where a Wigner 6$j$ symbol is used, and it is explicitly stated that only states with the same $F$ and $M_F$ are coupled by $\mathbf{H_Q}$. The last two angular bracketed quantities are reduced matrix elements.

The reduced matrix elements of $-\mu\cdot\mathbf{E}$ in the coupled basis are obtained with the aid of the following equation (after 5.72 [20]):

$$\langle\{J'I\}KF'||-\mu^{(1)}\cdot\mathbf{E}||\{JI\}KF\rangle = (-1)^{J'+I+F}\mu E[(2F'+1)(2F+1)]^{1/2}\begin{Bmatrix} J' & F' & \mathrm{I} \\ \mathrm{F} & \mathrm{J} & 1 \end{Bmatrix}\langle J'K||P_1||JK\rangle \quad (10)$$

where it is seen that $\mu\cdot\mathbf{E}$ can couple states with different $J$ and $F$.

Equations 9 and 10 are easily evaluated once the reduced matrix elements are known; however, obtaining the correct reduced matrix elements is often the most troublesome aspect of working with spherical tensors. Of course the key to assignment of reduced matrix elements is the Wigner−Eckart theorem. Here we write Zare's eq 5.14 to specify this theorem:

$$\langle\alpha'J'M'|T^k_q|\alpha JM\rangle = (-1)^{J'-M'}\begin{pmatrix} J' & k & \mathrm{J} \\ -\mathrm{M}' & \mathrm{q} & M \end{pmatrix}\langle\alpha'J||T^k||\alpha J\rangle \quad (11)$$

The Wigner−Eckart theorem can now be used to evaluate the necessary reduced matrix elements. The reduced matrix element of $V^2$ is the most perhaps the most difficult because the electric field gradient at the nucleus is specified with a value, $eq/2$, along the molecular axis that rotates with the molecule. The projection of this field gradient must be found on the space fixed $ZZ$ axis. With this in mind the reduced matrix element of $V^2$ is found after several steps after first recognizing that the quantum number $\alpha$ in eq 11 must be $K$. Then

$$\langle J'Km'|V^2_0|JKm'\rangle = \frac{eq}{2}\langle J'Km'|P_2|JKm'\rangle \quad (12)$$

where $m' = \min(J',J)$. Now using the Wigner−Eckart theorem and eq 4, it is easy to derive that

$$\langle J'K||V^2||JK\rangle = \frac{1}{2}eq(-1)^{K+J'}[(2J+1)(2J'+1)]^{1/2}\begin{pmatrix} J' & 2 & J \\ -K & 0 & K \end{pmatrix} \quad (13)$$

The reduced matrix element of $Q^{(2)}$ is easier because the nuclear quadrupole moment, $Q/2$, is already defined with respect to the space fixed $ZZ$ axis. We have immediately from the Wigner−Eckart theorem (with $M_I = I$ ) that

$$\langle I||Q^2||I\rangle\begin{pmatrix} \mathrm{I} & 2 & I \\ -I & 0 & I \end{pmatrix} = \frac{Q}{2} \quad (14)$$

The reduced matrix element of $Q^{(2)}$ is often written simply as[15]

$$\langle I||Q^2||I\rangle = \frac{Q}{2}\left[\frac{(2I+1)(I+1)(2I+3)}{I(2I-1)}\right]^{1/2} \quad (15)$$

The last reduced matrix element that we need is

$$\langle J'K||P_1||JK\rangle = (-1)^{K+J'}[(2J+1)(2J'+1)]^{1/2}\begin{pmatrix} J' & 1 & J \\ -K & 0 & K \end{pmatrix} \quad (16)$$

and then the matrix elements of $-\mu\cdot\mathbf{E}$ can be evaluated with the Wigner−Eckart theorem as

$$\langle\{J'I\}KF'M_F|-\mu\cdot\mathbf{E}|\{JI\}KFM_F\rangle = (-1)^{F'-M_F}\begin{pmatrix} F' & 1 & F \\ -M_F & 0 & M_F \end{pmatrix}\langle\{J'I\}KF'||-\mu^{(1)}\cdot\mathbf{E}||\{JI\}KF\rangle \quad (17)$$

Matrix elements of $\mathbf{H}$ are easily evaluated with the preceding formulas. In addition to the diagonal and off-diagonal contributions of $\mathbf{H_Q}$ and $-\mu\cdot\mathbf{E}$, the $\langle\{J'I\}KF'M_F|\mathbf{H}_0|\{JI\}KFM_F\rangle$ elements have nonzero values only for the diagonal elements where $J' = J$ and $F' = F$. These diagonal elements have the values, $hcBJ(J+1) + hc(A\text{-}B)K^2$. The above formulas have been checked by expanding the 3$j$ and 6$j$ symbols in their algebraic form and comparing them with the equations in Gordy and Cook.[21]

We conclude this section with the observation that other interactions of external fields with molecules can be handled with the equations of this section. In particular the interaction of the gradient of an applied electric field with the electric quadrupole moment of a symmetric top molecule can be evaluated with eq 4 for the case in which hyperfine interactions are neglected. The spherical tensor formalism will allow evaluation of matrix elements for this case when hyperfine interactions are not neglected.

**2.2. Trajectories.** The main goal of this paper is to explore the trajectories of symmetric top molecules in more or less axially symmetric electric fields. We treat the motion in ideal or approximate hexapole fields, because such trajectories are necessary for modeling molecular beam experiments. The ideal hexapole electric fields are axially symmetric, but experimental implementations commonly use cylindrical rods with the diameter of the rods equal to the radius, $r_0$, of the hexapole which is half of the distance between the inside surfaces of rods on opposite sides of the hexapole. We will see that the electric field of this approximate hexapole has significant deviations from axial symmetry.

To allow convenient calculation with electric fields that deviate from axial symmetry and to follow trajectories that do not have simple radial motion, we use Cartesian coordinates, $x$ and $y$, to describe the motion in planes perpendicular to the axis of the hexapole ($z$). We need to be able to follow the classical trajectory of a molecule that enters the hexapole field at the position $(x_0, y_0)$ with velocities $v_{x0}$, $v_{y0}$, and $v_z$ in order to find the exit position $(x_l, y_l)$ and exit velocities $v_{xl}$, $v_{yl}$, and $v_z$ after traversing length $l$ of the hexapole. We assume that $v_z$ is constant, that molecules disappear (pumped away) when they have a radius greater than $r_0$, and that there is no scattering by background gas within the hexapole (high-vacuum operating conditions). We also neglect the hexapole fringing electric fields.

The classical trajectories are described by Newton's equations as

$$\frac{\mathrm{d}^2x}{\mathrm{d}t^2} = \frac{-1}{m}\frac{\partial W}{\partial x}$$

$$\frac{\mathrm{d}^2y}{\mathrm{d}t^2} = \frac{-1}{m}\frac{\partial W}{\partial y} \quad (18)$$

where $W$ is defined by eq 2 and $m$ is the mass of the symmetric top molecule. Now the interaction energy is a function of $E$ and various molecular parameters and quantum numbers, so it is useful to write the trajectory equations as

$$\frac{\mathrm{d}^2x}{\mathrm{d}t^2} = \frac{-1}{m}\frac{\mathrm{d}W}{\mathrm{d}E}\frac{\partial E}{\partial x}$$

$$\frac{\mathrm{d}^2y}{\mathrm{d}t^2} = \frac{-1}{m}\frac{\mathrm{d}W}{\mathrm{d}E}\frac{\partial E}{\partial y} \quad (19)$$

where the partial derivative is evaluated at $(x, y)$ and the ordinary derivative is evaluated at $E(x, y)$. The forces that the molecule experience depend on the functional form of the interaction energy as a function of the electric field and on the functional

form of the electric field as a function of position. The trajectory equations must be integrated for $t$ between $t = 0$ and $t = l/v_z$.

The results of the previous section can be used to find the derivative of the interaction energy, $W$, with respect to $E$. First we consider the case where $\mathbf{H_Q}$ is neglected. If the interaction energy can be described by first order perturbation theory (linear Stark effect) then eq 5 gives

$$\frac{dW^{(1)}}{dE} = -\mu\frac{MK}{J(J+1)} = \langle\cos\theta\rangle \tag{20}$$

Second order perturbation theory gives a contribution to the derivative from by eq 6 that is linear in $E$ or $\Omega$:

$$\frac{dW^{(2)}}{dE} = \mu\Omega\left[\frac{[J^2-K^2][J^2-M^2]}{J^3(2J-1)(2J+1)} - \frac{[(J+1)^2-K^2][(J+1)^2-M^2]}{(J+1)^3(2J+1)(2J+3)}\right] \tag{21}$$

For the exact calculation of $W$ the derivative of $W$ with respect to $E$ can be evaluated with the help of the Hellman−Feynman theorem, but the trajectory calculations use the derivatives for many $E$, so it is easier to first accurately approximate the dependence of $W$ on $E$ with a series of Chebyshev polynomials[22] and then differentiate this series term by term to produce another Chebyshev series[22] for d$W$/d$E$. In this work it has been found that only ten terms in the Chebyshev series for the derivative are necessary to accurately compute d$W$/d$E$ for the exact Stark effect for the lowest energy states of $CH_3$ I with electric fields from 0 to 40 kV/cm. The first term gives d$W$/d$E$ for the linear Stark effect, and the first two terms yield the quadratic Stark effect. The coefficients of the polynomials are evaluated from the values of $W$ at 50 values of $E$.

The Chebyshev expansion technique also works well for the interaction energy for $CH_3I$ when $\mathbf{H_Q}$ is included. However for this case two Chebyshev series are used to accurately approximate $W$. The coefficients of one series are found with 50 values of $E$ from 0 to 1.5 kV/cm and the other with 50 values of $E$ from 1 to 40 kV/cm. Twenty terms are used for each series, and d$W$/d$E$ is evaluated with the first series for $E < 1.25$ kV/cm and the second for greater fields.

For the ideal hexapole field, the electric field is axially symmetric and has the magnitude

$$E(r) = \frac{3U_0}{r_0}\left(\frac{r}{r_0}\right)^2 \tag{22}$$

where $U_0$ is the half of the voltage difference between two hexapole rods. We see that the maximum electric field occurs for $r = r_0$ and has the magnitude $3U_0/r_0$. For the field represented by eq 22, the partial derivatives with respect to $x$ and $y$ are easily given as

$$\frac{\partial E}{\partial x} = \frac{6U_0}{{r_0}^3}x$$

$$\frac{\partial E}{\partial y} = \frac{6U_0}{{r_0}^3}y \tag{23}$$

If $W$ is accurately given by the linear Stark effect, and if the product $MK$ is negative, then both the $x$ and $y$ motions will be harmonic. This observation has been the basis of experimental methods for focusing symmetric top molecules in hexapole fields for more than 30 years. We can now proceed to examine the range of validity for the linear Stark effect and to see how deviations from the linear Stark effect will affect focusing. We will see that both strong fields and inclusion of hyperfine coupling make significant changes in the forces that molecules experience in hexapoles.

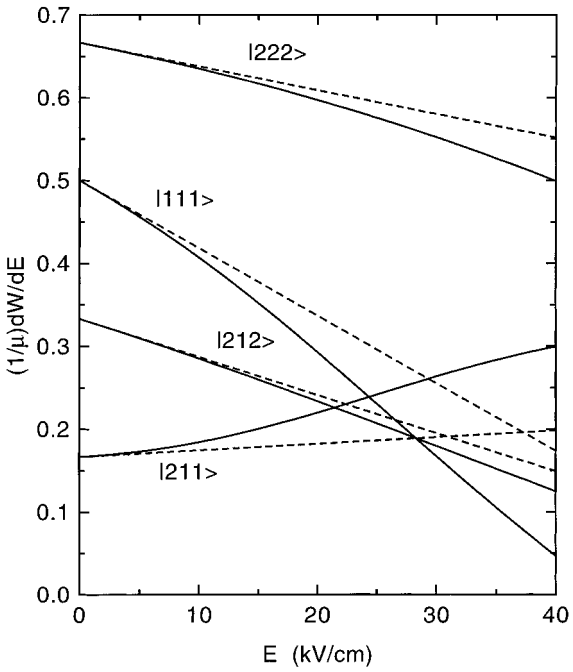


**Figure 1.** Effective force constants for exact and second order Stark effects (eqs 20 and 21 in text) for the |111⟩, |211⟩, |212⟩, and |222⟩ states of $CH_3I$. The solid lines indicate the exact interaction, and the dashed lines indicate the interaction to second order.

## 3. Results

**3.1. Forces in Ideal Hexapole Fields.** Since there is a simple linear restoring force for a molecule with a linear Stark effect in an ideal hexapole field, we will now compare the actual force that a molecule will experience (exact calculation of the interaction energy) with the force for the linear Stark effect. Figures 1 and 2 give this comparison for the case in which $\mathbf{H_Q}$ is neglected in $CH_3$ I. These figures use recent literature values for $B$ and $\mu$ [15] for the quadratic Stark effect and the exact calculations. Thirty (30) basis functions (different $J$ ) are used. Figure 1 gives results for the |111⟩, |211⟩, |212⟩, and |222⟩ states, and Figure 2 gives results for the |311⟩, |312⟩, |313⟩, and |323⟩ states. The notation used here actually gives the absolute value for each quantum number ($K$ and $M$ ), but the understanding is that the product $MK$ is negative so the |111⟩ state could be |1 − 1 1⟩ or |1 1 − 1⟩. If the linear Stark effect were valid for all $E$, then eq 20 shows that each state would have the exact interaction (solid line) as a horizontal line with $(1/\mu)(dW/dE) = -MK/[J(J+1)]$. However, all of the states with the exception of the |312⟩ state show significant deviation from the linear Stark effect expectation.

The figures also show the expected results (dashed straight lines) when the quadratic Stark contribution (eq 21) is included with the linear Stark effect. The figures show that there are significant deviations from the quadratic Stark effect for $E$ of about 5 kV/cm for the |111⟩ and |211⟩ states, but that the quadratic Stark effect provides a good approximation for states with $J = 3$. As expected the exact and second order Stark interactions show the same deviation (increasing or decreasing) with increasing $E$. We will see the consequences of positive or negative deviations when we present the results of trajectory calculations.

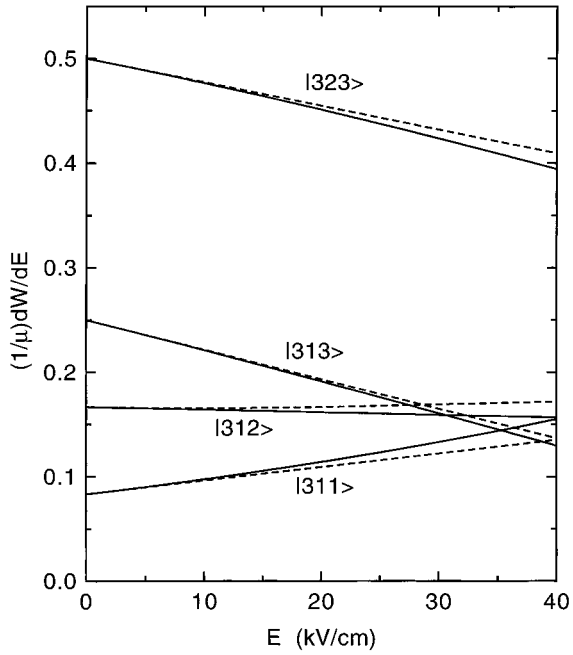


**Figure 2.** Effective force constants for exact and second order Stark effects for the |311⟩, |312⟩, |313⟩, and |323⟩ states of $CH_3I$. Solid and dashed lines are as in Figure 1.

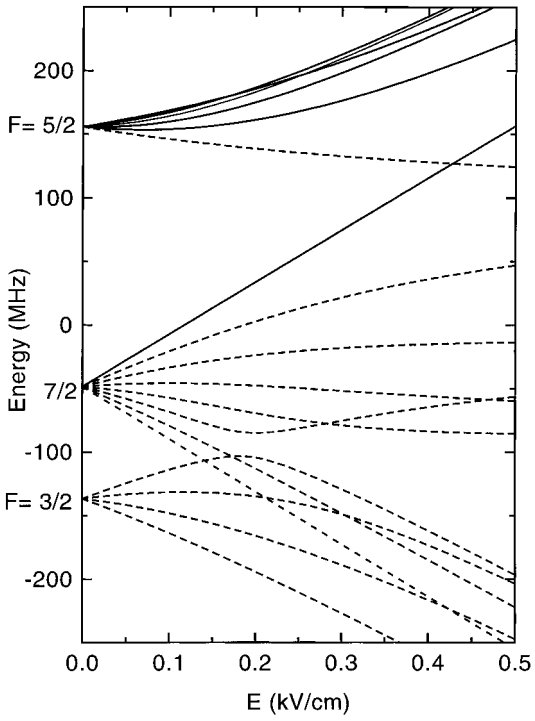


**Figure 3.** Exact Stark interaction energies for $CH_3I$, including the nuclear quadrupole−electric field gradient interaction for the I nucleus. This diagram is drawn for the lowest energy states (nominally |111⟩), and the $F$ values are indicated. The states that can be focused in hexapole electric fields are indicated by solid lines. The states that cannot be focused are indicated by dashed lines.

The force that a molecule experiences when the nuclear quadrupole−electric field gradient interaction is included can also be calculated. Here we use the nuclear quadrupole−electric field gradient parameter (eqQ = −1934.0995 MHz) used by Bulthuis *et al.*[15] and 50 basis functions (different $J$ and $F$ ). Figure 3 shows the interaction energy for the lowest states of $CH_3I$ with $K = -1$ and $M_F$ having values ranging from $-^7/_2$ to $+^7/_2$ (note the that the same curves apply for $K = 1$ when one switches the sign of the $M_F$ labels!). This set of $M_F$ values

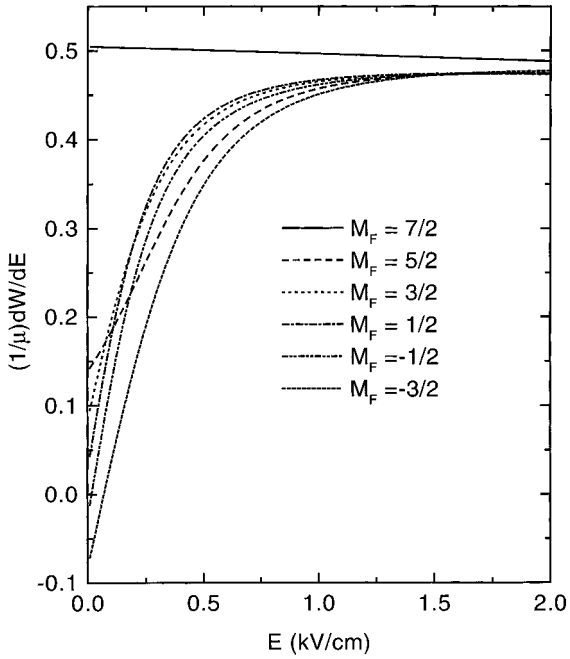


**Figure 4.** Effective force constants for the states in Figure 3 that can be focused.

gives the expected 18 states for the lowest $F = ^3/_2$, $F = ^5/_2$, and $F = ^7/_2$ states. The energies of the states are referred to the zero field mean of the state energies and agree very well with other results.[15] The main differences with this work and the earlier work[15] is that they used the uncoupled representation and also included nuclear spin effects for all nuclei. Inclusion of the other nuclei changes the set of $F$ and $M_F$ quantum numbers and also gives rise to a number of near or real crossings that have energy splittings that are too small to effect the parentage of a $CH_3I$ state as it travels through a hexapole.

Figure 3 uses solid lines to indicate the states that correlate with the focusable state |111⟩ for the case in which nuclear quadrupole−electric field gradient interactions are neglected. There are six, $(2I + 1)$, such states with $M_F$ values that range from $-^3/_2$ to $+^7/_2$ in unit increments. The $M_F = ^7/_2$ state arises from the $F = ^7/_2$ states, while the others arise from the $F = ^5/_2$ states. The two states with $|M_F| = ^7/_2$ show linear Stark effects, and this is simply due to the fact that they do not couple with any of the other $J = 1$ states. The other five focusable states with $M_F$ having values from $-^3/_2$ to $+^5/_2$ definitely show significant deviations from the linear Stark effect at the relatively small electric fields shown in this figure.

Figure 4 shows the effect of $\mathbf{H_Q}$ on the force that a $CH_3I$ molecule experiences in a hexapole field. Not surprisingly the $M_F = ^7/_2$ state focuses very much like the $M_J = 1$ state would focus without nuclear quadrupole coupling, but it is interesting to note that the linear Stark effect force is actually about 1% larger than it would be without the nuclear quadrupole coupling. This is because $\mathbf{H_Q}$ couples together different $J$ even in the zero field limit, and the electric field matrix elements add with definite phases to these zero field matrix elements. The other $M_F$ show less and less focusing for small $E$ as $M_F$ decreases. We note that $M_F = -^1/_2$ and $M_F = -^3/_2$ show defocusing for small applied electric fields. We will see that this low-field behavior of the forces when $\mathbf{H_Q}$ is included makes significant differences in the transmission of a hexapole.

**3.2. Trajectory Results.** This section presents the results of trajectory calculations for different states of $CH_3$ I with neglect or inclusion of $\mathbf{H_Q}$. The hexapole is assumed to have an ideal hexapole electric field: length, $l = 200$ cm, and radius,

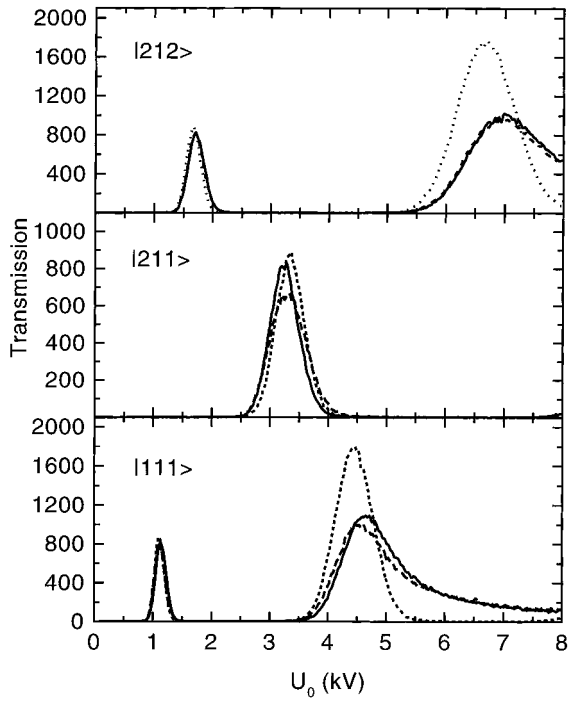


**Figure 5.** Transmission of an ideal hexapole electric field for the |111⟩, |211⟩, and |212⟩ states of $CH_3I$ neglecting the nuclear quadrupole interaction. The solid lines represent the focusing due to the exact interaction. The dotted and dashed lines represent the focusing for the Stark effect calculated to first and to second order, respectively.

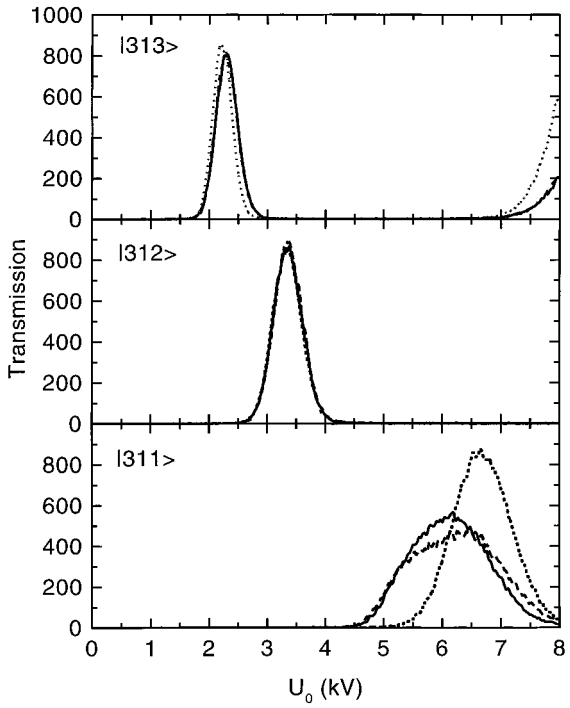


**Figure 6.** Transmission of an ideal hexapole electric field for the |311⟩, |312⟩, and |313⟩ states of $CH_3I$ neglecting the nuclear quadrupole interaction. The solid lines represent the focusing due to the exact interaction. The dotted and dashed lines represent the focusing for the Stark effect calculated to first and to second order, respectively.

$r_0 = 0.7$ cm. At the highest rod voltage, $U_0$, the maximum electric field is 34.3 kV/cm. The initial positions, $x_0$ and $y_0$, are randomly chosen within a circle with radius = 0.005 cm, and the velocity, $v_x$, is chosen from a Gaussian velocity distribution centered at 300 m/s with a velocity width corresponding to a translational temperature of 2 K. The velocities, $v_{x0}$ and $v_{y0}$, are given random values between $-0.06\ v_z$ and $+0.06\ v_z$. A molecule is transmitted through the hexapole if it never has a radial displacement in the hexapole greater than $r_0$ and it leaves the hexapole with $x_l^2 + y_l^2 \leq 0.005$ cm. Equations 19 are integrated with a fourth order Runge−Kutta routine[22] for all orders of the Stark effect. Good accuracy results with 24 integration steps over the length of the hexapole. Runge−Kutta integration is not necessary for the simple harmonic motion that characterizes the linear Stark effect, but it is convenient to use the same integration routine for all cases.

Figure 5 shows trajectory results for the |111⟩, |211⟩, and |212⟩ states of $CH_3I$ if $\mathbf{H_Q}$ is neglected. Figure 6 shows the trajectory results for the |311⟩, |312⟩, and |313⟩ states. Each focusing curve is calculated with 100 000 trajectories calculated at each of 800 values for $U_0$ separated by 0.01 kV. The focusing curves are presented with enough smoothing to allow easy differentiation. The results show that the maximum transmission (one wavelength focus) for this hexapole implementation would be about 2% if the first order Stark effect were valid. The transmission is defined as the number of molecules that pass through the exit aperture divided by the number that satisfy the initial conditions for position and velocity. In each plot the exact focusing curve is the solid line, the linear Stark effect focusing is shown with a dotted line, and the quadratic Stark effect focusing is shown with a dashed line. It is interesting to note that the focused molecules have a very large increase in their intensity over that expected from the solid angle subtended by the exit aperture of the hexapole. If focusing were not present, we would expect a transmission of only $1.36 \times 10^{-5}$%, so the intensity enhancement is 150 000. Similar enhancements for a different hexapole geometry have been obtained by Harren *et al.*[13]

The |111⟩ and |212⟩ states show similar differences between the focusing for the exact and linear Stark effects. Both of these states show two peaks in the focusing curves over this $U_0$ range. The lower voltage focus corresponds to a "half-wavelength" focus criterion, where the molecule does not cross the axis of the hexapole as it travels through. The higher $U_0$ focus corresponds to to a "one wavelength" focus criterion, where focused trajectories cross the axis of the hexapole at $z = l/2$. Generally the one wavelength foci have larger intensity than the half-wavelength foci, because the former correspond to larger angular divergence of the incident beam (larger transverse velocities). In some cases there are trajectories with $^3/_2$ or more "wavelengths". However, beam stops are often placed at various positions interior or exterior to hexapoles to help prevent unwanted transmission of molecules that are not focused. If a beam stop were located at $z = l/2$, it would stop the transmission of one wavelength focused molecules.

The linear Stark effect is more strongly focusing than the exact Stark effect for both the |111⟩ and |212⟩ states, and there is very little difference for the focus at low $U_0$. The stronger focusing and the lack of differences for the low-$U_0$ focus is consistent with the data in Figure 1. For $U_0 = 2$ kV the maximum electric field is 8.6 kV/cm, and Figure 1 shows that the linear and exact forces differ for this electric field by about 10%. The |211⟩ state has stronger focusing with the exact Stark effect, and this is again consistent with Figure 1. Figure 1 also indicates that the force for given $E$ that acts on a |211⟩ molecule is less than that operating on a |111⟩ or |212⟩ molecule. Hence the half-wavelength focus for |211⟩ occurs at higher $U_0$ values.

Figure 5 also shows that the one wavelength focus is quite different for the linear and the exact Stark effects. The peak transmission for the exact interaction is much lower than that for the linear Stark effect. Also the exact transmission peak

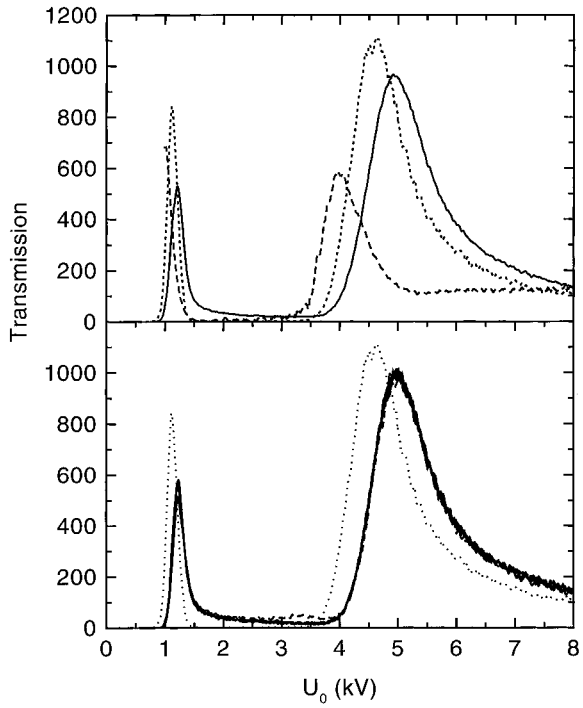


**Figure 7.** Transmission of the lowest energy states of $CH_3I$ in an ideal hexapole electric field including the nuclear quadrupole interaction. The bottom panel shows the transmission for each $M_F$ state, and the essentially uncoupled $M_F = {}^7/_2$ state is indicated with a dotted line. All of the other $M_F$ states are indicated with solid lines. The $M_F = {}^5/_2$ state is responsible for the small peak at 3.4 kV/cm. The top panel compares the $M_F = {}^7/_2$ transmission (dotted line) with the average of all $M_F$ states (solid line). The dashed line in the upper panel shows 10 times the percentage of the total transmitted beam that is in the $M_F = {}^7/_2$ state.

has a large width and a long tail toward higher $U_0$. The width of the transmission peaks for the linear Stark effect is due to the velocity spread of the molecular beam (chromatic aberration), but the additional broadening for the exact treatment is due to the angular spread of the molecular beam (spherical aberration). Molecules with large transverse velocities sample the high-field parts of the hexapole where the forces are definitely not harmonic. The amount of tailing at the high-$U_0$ values will be significantly determined by the exact collimation that is used in a particular experiment.

Figure 6 shows many of the same trends as Figure 5. However, the $|311\rangle$ and $|312\rangle$ states are interesting. The $|311\rangle$ state has its half-wavelength focus at high fields, and this state is more strongly focused in the exact Stark effect than in the linear approximation. Now the exact peak is significantly broadened, but it maintains good symmetry. The $|312\rangle$ state shows very little difference between the exact and linear Stark effect forces in Figure 2. This is very evident in the near superposition of the focusing curves in Figure 6.

Figures 5 and 6 also show that there are differences between focusing calculated with the exact Stark effect and that calculated including terms to second order in the Stark effect. The differences are particularly marked for the $|111\rangle$, $|211\rangle$ states and the $|311\rangle$ state. The peak position, width, shape, and magnitude may differ. However, there is little difference between the exact and quadratic Stark trajectories for the $|212\rangle$ state, although there is a large difference between the first order and exact calculations for the one wavelength trajectories. This is consistent with the data in Figure 1 for this state.

Focusing curves can also be determined including the effects of $\mathbf{H_Q}$, and such results are shown in Figure 7. The lower panel indicates the differences in the focusing curves for the different $M_F$ states that correspond to the $|111\rangle$ state without hyperfine interactions. The $M_F = {}^7/_2$ state focuses differently from the other five $M_F$ states. This focusing difference is not surprising considering the results presented in Figure 4. The $M_F = {}^7/_2$ state behaves as if there were no hyperfine interaction. The lower panel in Figure 7 shows that there is a significant shift to higher $U_0$ in the transmission peaks for the states with $M_F \neq {}^7/_2$. There is also significant tailing of the transmission to the high-$U_0$ side of the half-wavelength peak, and the $M_F = {}^5/_2$ state is responsible for the small maximum at $U_0 = 3.4$ kV.

The top panel of Figure 7 compares the $M_F = {}^7/_2$ focusing curve with the average of the curves for all six focusable $M_F$ states. For $U_0$ on the rising edge of the focusing peaks the transmission will favor the $M_F = {}^7/_2$ state. This gives the possibility of producing a partially nuclear spin polarized molecular beam of $CH_3I$. The dashed line gives the percentage of spin polarized $CH_3I$, and useful transmitted beam intensity can be obtained with more than 40% in the $M_F = {}^7/_2$ state.

**3.3. Cylindrical Rod Approximation for Hexapole Fields.** The trajectory results of the last section used an ideal hexapole electric field. However, most experiments use hexapoles constructed with cylindrical rods of diameter equal to half of the radius, $r_0$ of the hexapole or with rod radius, $\rho_0 = 0.5r_0$. This choice for the rod radius makes the curvature of the ideal hexapole electric field equal to the curvature of the rods at $r_0$.[5] We can now investigate the implications of this approximation for hexapole fields.

First we must find the electric field distribution for the cylindrical rod configuration. The straightforward approach to this task is to first solve the Laplace equation:

$$\frac{\partial^2 V}{\partial x^2} + \frac{\partial^2 V}{\partial y^2} = 0 \tag{24}$$

where $V$ is the potential at the point $(x, y)$. Then the electric field components, $E_x$ and $E_y$, can be calculated as follows: $E_x = \partial V/\partial x$ and $E_y = \partial V/\partial y$. The Laplace equation can be solved with an expansion in Bessel functions, but it is easier to seek a finite difference solution. Here a grid with 801 points on a side was used to find the potential distribution. This corresponds to a maximum radius within the square box of 400 points. Initially the potential is specified by setting the potential to 0 for all points with radius greater than or equal to 400 and the points corresponding to the cylindrical rod positions alternately to the potential $+1$ or $-1$. Additionally the potential at the origin is set to $V = 0$. The centers of the rods (of radius = 80 grid units) are found on a circle of radius = 240 grid units. This leaves the radius, $r_0$, of the hexapole to be 160 grid units. The resulting potential is for a hexapole field with a grounded surface at $2.5r_0$, but previous work[19,23] indicates that the potential within a hexapole or quadrupole is not significantly affected by the location of the grounded surface. The finite difference equations are solved by the simultaneous over relaxation (SOR) technique[22] to give the potential at each grid point.

The electric field components are determined with the symmetric finite difference approximation for partial derivatives (care must be taken to avoid points of fixed potential), and the electric field magnitude is found as $E = [E_x^2 + E_y^2]^{1/2}$. The magnitude of the electric field is plotted as a contour plot in Figure 8. The plot shows that the magnitude of the electric field shows good axial symmetry for $r/r_0$ less than 0.5, but that significant deviations appear for larger $r/r_0$. In particular the flattening of the contours indicate that there will be significant tangential forces acting on a molecule with a linear Stark effect. This finite difference approximation for the magnitude of the electric field was used early in this work for trajectory

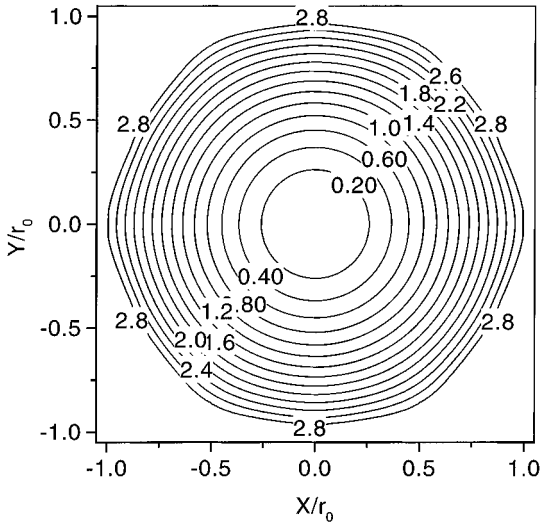


**Figure 8.** Magnitude of the electric field for a hexapole constructed of cylindrical rods with radius $\rho_0 = 0.5r_0$. The cylinders are found where the contours are labeled "2.8". The units of the electric field are $U_0/r_0$.

calculations, but the trajectory calculations presented below use a function of $r$ and $\theta$ that is fitted to the finite difference results. This function is the following:

$$E(r,\theta) = \frac{U_0}{r_0}\left(\frac{r}{r_0}\right)^2\left[2.9498398 - 0.1122901\left(\frac{r}{r_0}\right)^6\cos(6\theta) - 0.0376238\left(\frac{r}{r_0}\right)^{12}\cos(12\theta)\right] \quad (25)$$

Equation 25 provides a good fit to the electric field distribution with a fractional error of only 0.1% of the maximum field values. If only the first term is used, the fractional error is 0.7%, and using two terms has an error of 0.2%. Other authors[19,23] have fitted the radial and angular dependence of the potential for multipole fields with expressions similar to eq 25, but for this work fits to the electric field magnitude were done because the field is everywhere positive and more slowly varying than the potential. For the actual calculations of trajectories eq 25 is written in terms of the Cartesian equivalents of $\theta$ and $r$. For example $r^3\cos(3\theta) = x^3 - 3y^2x$.

Vonbun[24] has derived equations to treat the electric field distribution for 2$n$-pole devices that use cylindrical rods. However, his electric fields differ significantly from the fields calculated here. There is a cautionary remark in his paper that says that the equations will only be good for rod radii, $\rho_0$, that are small with respect to $r_0$. Apparently rod radii that are half of $r_0$ are too large for his equations to be accurate.

Figure 9 shows focusing curves for the |111⟩, |212⟩, and |313⟩ states of $CH_3I$, neglecting $\mathbf{H_Q}$ for ideal and cylindrical rod hexapoles. The ideal hexapole focusing curves are shown as solid lines, and the calculations for $\rho_0 = 0.5r_0$ and $\rho_0 = 0.565r_0$ are shown as dotted and dashed lines, respectively. The focusing curves show that cylindrical rod hexapoles have the interesting feature that the peaks are more symmetrical than they would be in ideal hexapoles. However, the overall transmission for a hexapole constructed with cylindrical rods with $\rho_0 = 0.5r_0$ is significantly smaller than that for an ideal hexapole. The focusing curves for a hexapole constructed with cylindrical rods with $\rho_0 = 0.565r_0$ have less difference from those for the ideal hexapole. It is interesting to note that the peaks occur at the same position for all of these hexapoles. This figure shows that $\rho_0 = 0.5r_0$ cylindrical rod hexapoles are likely to be preferred, because generally in state selective studies to yield oriented molecules narrow symmetric peaks are more important than slightly larger, but broader and less symmetric, peaks.

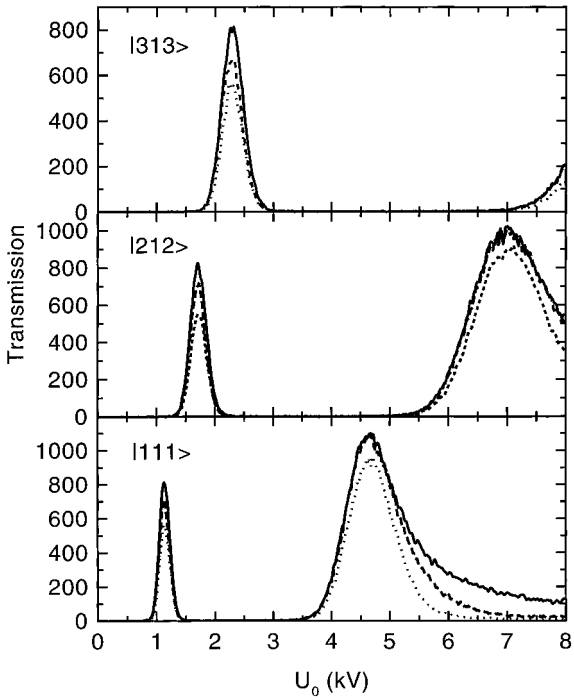


**Figure 9.** Transmission of the |111⟩, |212⟩, and |313⟩ states of $CH_3I$ for exact Stark interaction with neglect of nuclear quadrupole coupling in ideal hexapole fields (solid lines) and in two cylindrical rod approximations: $\rho_0 = 0.5\ r_0$ (dotted lines) and $\rho_0 = 0.565r_0$ (dashed lines).

## 4. Discussion

The preceding results show that serious errors may occur if only the first order Stark effect is considered for trajectories in hexapole fields. Errors may also occur if the Stark effect is calculated only to second order. It is important to evaluate the electric field−dipole interaction to high order and to consider the effects of nuclear quadrupole moment−electric field gradient couplings for molecules with heavy nuclei. The use of cylindrical rods for hexapole construction can also give quite different focusing curves than ideal hexapoles.

In this discussion we will first consider the application of some of the results of this paper to the experimental hexapole arrangement of Ohoyama *et al.*.[12] To do this, a computer program in Fortran has been written that calculates focusing curves with user specification of the order for the Stark effect and with user specification of experimental conditions. The program allows the user to specify a point source at a distance $z = 0$ which may be either on axis or at an off-axis position ($x_0$,$y_0$ ). The user can also specify the $z$ axis position and dimensions of on-axis collimation apertures (circular or rectangular) before and/or after the hexapole. The $z$ position of the start and end of the hexapole as well as its $r_0$ can be specified. Finally the program allows specification of up to three beam stops ($z$ position, and circular or rectangular dimensions). One beam stop can be specified before the start of the hexapole, another within the hexapole, and the third between the end of the hexapole and the detector or interaction region. The program allows specification of velocity distributions of the form

$$f(v) = v^n \exp\left(\frac{-m(v - v_0)^2}{2kT}\right) \quad (26)$$

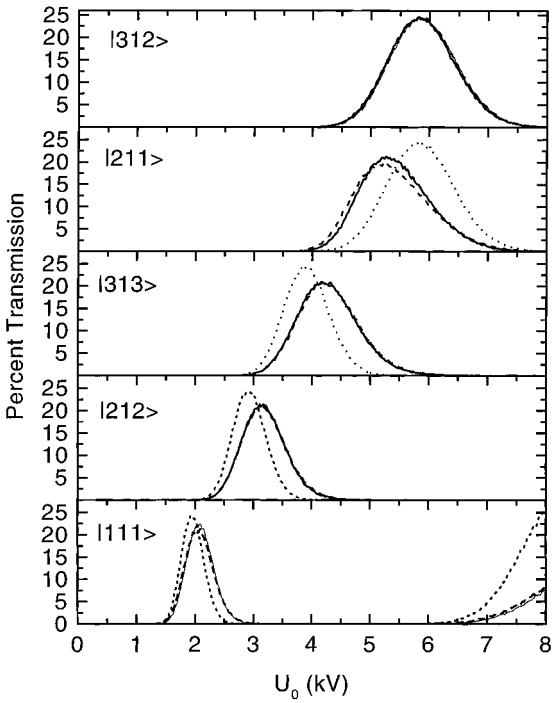


**Figure 10.** Transmission of a hexapole focusing arrangement for $CH_3I$ with the experimental dimensions of ref 12. The dotted and dashed lines assume focusing calculated with the Stark effect calculated to first and to second order, respectively. The solid lines show the focusing for the exact Stark effect. Hyperfine interactions and the effects of the cylindrical rod approximation to the hexapole field are neglected.

where $n$, $m$, $v_0$, and $T$ can be specified. Copies of this program can be obtained via e-mail from the author.

Figure 10 shows the focusing curves for several states of $CH_3I$ using the hexapole, collimation, and molecule speed parameters of Ohoyama *et al.*[12] For these experiments one beam stop is placed before the hexapole, and this beam stop blocks some of the "half-wavelength" trajectories. Figure 10 shows focusing curves calculated with the exact Stark effect and with the Stark effect calculated to first and to second order. The transmission for these experimental simulations is defined as the number of molecules that pass through the detector aperture divided by the number of molecules that would pass through the initial collimating aperature if the beam stop were not present. These curves can be compared with the calculations for second order and linear Stark effects in ref 12 (Figure 4). We expect that the present results for the linear and quadratic Stark effect should agree with those of Ohoyama *et al.* However, the linear Stark focusing peaks of Ohoyama *et al.* are only 70% of the size for those in the present work. The reason for this discrepancy is that the angular distribution of molecules entering the hexapole is incorrectly estimated by Ohoyama. Ohoyama *et al.* perform the angular integration without the sin $\theta$ solid angle factor that accounts for the fact that there are more molecules entering with off-axis angles between $\theta$ and $\theta + d\theta$ for larger $\theta$. With the Ohoyama *et al.* experimental arrangement the inclusion of the correct angular averaging makes a large effect because molecules can only be transmitted through the hexapole if they have large enough angles to go around the beam stop. This averaging problem makes it difficult to compare the present linear, quadratic, and exact Stark effect calculations with the linear and quadratic results of Ohoyama *et al.*. However, we can make some remarks about the present results in Figure 10. There is very little difference between the quadratic and exact focusing curves for the $|212\rangle$, $|313\rangle$, and $|312\rangle$ states. Some difference can be seen for the $|111\rangle$ state, and the most difference is seen for the $|211\rangle$ state. For this experimental arrangement the largest differences between the exact and second order calculations is seen for a state where the interaction is increased when higher order Stark effects are included. The linear and exact Stark effects for $|312\rangle$ give the same focusing curve, which can be easily explained by the results given in Figure 2. Figure 10 shows that it is important to use exact or high-order estimates for $W$ for this experimental arrangement. Significant errors are introduced if $W$ is calculated only to first order.

The difference between focusing curves that are calculated with the linear and exact Stark effects will depend on the experimental collimator positions and dimensions and on the position of the beam stops. If no beam stops are used with small collimators, there should be little difference between the linear and exact Stark trajectories because the molecules will always travel near the hexapole axis where the electric fields are small. If larger collimators are used without beam stops, results similar to those in Figures 5 and 6 should be obtained. The half-wavelength peaks at small values of $U_0$ should have less difference between the exact and linear Stark trajectories, and the peaks at larger $U_0$ should show larger differences between the linear and exact Stark trajectories. If a beam stop is inserted near the middle of the hexapole, it will tend to block one wavelength trajectories and the half-wavelength trajectories that are transmitted will tend be less influenced by the difference between the linear and exact Stark forces.

We have seen the hyperfine interactions can also significantly influence the trajectories of molecules in hexapole fields. Such interactions decrease the restoring force in small electric fields, so that there is less focusing whenever the molecules are near the hexapole axis. This observation is true for most of the $M_F$ states. However, the $M_F$ state with the largest value for a given $J$ focuses as if hyperfine interactions were not present. This allows the production of partially nuclear spin polarized beams, and it also explains why there is always some orientation that is preserved even with low guiding electric fields (see ref 15). However, we expect that the position of beam stops and the size of collimating apertures will affect the importance of hyperfine interactions on trajectories. If the collimation keeps all of the molecules near the hexapole axis, there should be a large effect of the hyperfine interactions on the focusing curves, because most of the molecular movement will be in regions of low applied electric field. However, if a beam stop is placed before the hexapole so that it blocks half-wavelength trajectories, the effects of the hyperfine interaction should be smaller because most of the trajectories will be in regions with larger electric fields.

The experimental simulations in Figure 10 ignore the effects of hyperfine interactions, and such interactions would clearly have importance for molecules such as $CH_3I$, especially in the $|111\rangle$ state where the rotational spacing is smallest.

The final comments in this discussion concern the construction of hexapoles with cylindrical rods. We have already seen that there are significant differences between exact Stark trajectories in ideal hexapoles and in cylindrical rod hexapoles where the radius of the rods, $\rho_0$, is half of the radius of the hexapole, $r_0$. The trajectories differ primarily because of the large coefficient of the $(r/r_0)^6 \cos(6\theta)$ term in eq 25. This choice for the value of $\rho_0$ is the most commonly used, but other values have been used. Kramer and Bernstein[2] used $\rho_0 = 0.667r_0$, and Everdij *et al.*[19] suggest using $\rho_0 = 0.56028r_0$. The latter value was obtained from an analysis like the one done earlier by Denison[23] for quadrupole electric fields. Denison observed that the magnitude of the $(r/r_0)^4 \cos(4\theta)$ term in the quadrupole electric field (expansion analogous to eq 25) depended on the

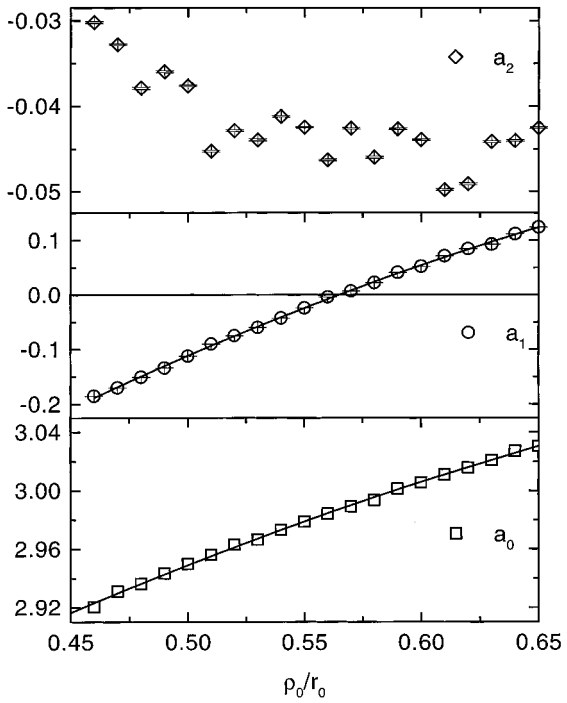


**Figure 11.** Coefficients in the expansion of the electric field magnitude for different cylindrical rod approximations for a hexapole field. The coefficients $a_0$, $a_1$, and $a_2$ are defined by eq 27. The lines drawn through the points for $a_0$ and $a_1$ are defined by eqs 29 and 28, respectively.

ratio of $\rho_0$ to $r_0$. In fact the coefficient of this term vanished for some value of the ratio. Everdij *et al.*[19] used the same argument for hexapole fields to deduce the ratio for which the $(r/r_0)^6 \cos(6\theta)$ will vanish.

Figure 11 presents the results of fits to the electric field for cylindrical rod hexapoles with $\rho_0$ to $r_0$ ratios between 0.46 and 0.65. The electric fields are fitted to the following equation:

$$E(r,\theta) = \frac{U_0}{r_0}\left(\frac{r}{r_0}\right)^2\left[a_0 + a_1\left(\frac{r}{r_0}\right)^6 \cos(6\theta) + a_2\left(\frac{r}{r_0}\right)^{12} \cos(12\theta)\right] \quad (27)$$

It is easily seen that the $a_1$ term will vanish for $\rho_0/r_0$ near 0.565. Figure 11 also shows a line for a fit to the values for $a_1$ for different values of the radius ratio. This fit is given by the following equation:

$$a_1 = (a + b(\rho_0/r_0))((\rho_0/r_0) - c) \quad (28)$$

The fit of this equation to the $a_1$ data yields $a = 2.61 \pm 0.10$, $b = -1.78 \pm 0.18$, and $c = 0.5650 \pm 0.0005$. It appears that $\rho_0$ should be 0.565 $r_0$ for the best approximation of a hexapole field with a cylindrical rod hexapole. This is close to the value given by Everdij *et al.*[19]

Figure 11 also gives the dependence of the $a_0$ term on the $\rho_0$ to $r_0$ ratio.

$$a_0 = (a + b(\rho_0/r_0) + c(\rho_0/r_0)^2) \quad (29)$$

where $a = 2.500 \pm 0.027$, $b = 1.171 \pm 0.096$, and $c = -0.546 \pm 0.087$. It is interesting to note that the $a_0$ term is equal to 3 for $\rho_0/r_0$ slightly greater than 0.6.

Finally values for $a_2$ are presented in Figure 11. Here although the values are precisely determined for given ratios of $\rho_0$ to $r_0$, the values for $a_2$ show some scatter from a simple curve. However, the plotted values should suffice for determining the appropriate values for this parameter that will represent the electric field magnitude for a given hexapole construction. The scatter in the values for $a_2$ may originate in the fact that a given grid for the finite difference calculation will not allow very precise definition of the cylindrical rod boundaries.

Figure 9 shows that hexapoles with $\rho_0 = 0.565r_0$ have focusing curves that more closely approximate focusing curves for ideal hexapoles than hexapoles with $\rho_0 = 0.5r_0$.

**Acknowledgment.** The author would like to thank the Zentrum für Interdisziplinäre Forschung at the Universität Bielefeld for their support and hospitality during this work. He would also like to acknowledge helpful and stimulating discussions with Professors K. Kuwata, N. Böwering, H.-J. Loesch, and J. Hinze in Bielefeld.

## References and Notes

(1) Bennewitz, H. G.; Paul, W.; Schlier, C. *Z. Phys.* **1955**, *141*, 6.
(2) Kramer, K. H.; Bernstein, R. B. *J. Chem. Phys.* **1965**, *42*, 767.
(3) Brooks, P. R. *Science* **1976**, *193*, 11.
(4) Stolte, S. *Ber. Bunsen-ges. Phys. Chem.* **1982**, *86*, 413.
(5) Reuss, J. In *Atomic and Molecular Beam Methods*; Scoles, G., Ed.; Oxford University Press: New York, 1988; Vol. I.
(6) Parker, D. H.; Bernstein, R. B. *Annu. Rev. Phys. Chem.* **1989**, *40*, 561.
(7) Loesch, H. J. *Annu. Rev. Phys. Chem.* **1995**, *46*, 555.
(8) Gandhi, S. R.; Curtiss, T. J.; Bernstein, R. B. *Phys. Rev. Lett.* **1987**, *59*, 2951.
(9) Xu, Q.-X.; Jung, K.-H.; Bernstein, R. B. *J. Chem. Phys.* **1988**, *89*, 2099.
(10) Böwering, N.; Volkmer, M.; Meier, C.; Lieschke, J.; Fink, M. *Z. Phys. D* **1994**, *30*, 177.
(11) Volkmer, M.; Meier, C.; Lieschke, J.; Mihill, A.; Fink, M.; Böwering, N. *Phys. Rev. A* **1996**, *53*, 1457.
(12) Ohoyama, H.; Ogawa, T.; Kasai, T. *J. Phys. Chem.* **1995**, *99*, 13606.
(13) Harren, F.; Parker, D. H.; Stolte, S. *Comments At. Mol. Phys.* **1991**, *26*, 109.
(14) Che, D.-C.; Ogawa, T.; Ohoyama, H.; Kasai, T.; Kuwata, K. *Bull. Chem. Soc. Jpn.* **1995**, *68*, 771.
(15) Bulthuis, J.; Milan, J. B.; Janssen, M. H. M.; Stolte, S. *J. Chem. Phys.* **1991**, *94*, 7181.
(16) Bulthuis, J.; Stolte, S. *J. Phys. Chem.* **1991**, *95*, 8180.
(17) Gandhi, S. R.; Curtiss, T. J.; Xu, Q.-X.; Choi, S. E.; Bernstein, R. *Chem. Phys. Lett.* **1986**, *132*, 6.
(18) Cho, V. A.; Bernstein, R. B. *J. Phys. Chem.* **1991**, *95*, 8129.
(19) Everdij, J. J.; Huijser, A.; Verster, N. F. *Rev. Sci. Instrum.* **1973**, *44*, 721.
(20) Zare, R. N. *Angular Momentum*; Wiley: New York, 1988.
(21) Gordy, W.; Cook, R. L. *Microwave Molecular Spectra*; Wiley: New York, 1970.
(22) Press, W. H.; Teukolsky, S. A.; Vetterling, W. T.; Flannery, B. P. *Numerical Recipes in Fortran*; Cambridge University Press: Cambridge, U.K., 1992.
(23) Denison, D. R. *J. Vac. Sci. Technol.* **1971**, *8*, 266.
(24) Vonbun, F. O. *J. Appl. Phys.* **1958**, *29*, 632.